Multiple spike time patterns occur at bifurcation points of membrane potential dynamics

P.J. Thomas[1], J. Vincent Toups[2], Jean-Marc Fellous[3], Terrence J. Sejnowski[4] and Paul Tiesinga[1,5],

[1]Departments of Mathematics, Biology and Cognitive Science, Case Western Reserve University, Cleveland, United States and Department of Neuroscience, Oberlin College, Oberlin, United States

[2]Computational Neurophysics Laboratory, Department of Physics & Astronomy, University of North Carolina, Chapel Hill, United States.

[3]Psychology Department and Program in Applied Mathematics, University of Arizona, Tucson, United States

[4]Computational Neurobiology Lab and Howard Hughes Medical Institute, Salk Institute, La Jolla, United States and Division of Biological Sciences, University of California at San Diego, La Jolla, United States

[5]Neuroinformatics, Donders Institute for Brain, Cognition and Behavior, Radboud University Nijmegen, Nijmegen, The Netherlands.

Introduction

The response of a neuron to fluctuating current injected in vitro often elicits a reliable and precisely timed sequence of action potentials when the same waveform is repeated. The response obtained across trials can be interpreted as the response of an ensemble of similar neurons, with the precise spike times representing synchronous volleys that would be effective in driving postsynaptic neurons. To study the reproducibility of the output spike times for different conditions that might occur in vivo, we somatically injected an aperiodic current into cortical neurons in vitro and varied the amplitude of the fluctuations and the constant pedestal or offset. As the amplitude of the fluctuations was increased the spike reliabilities increased and the spike times remained stable over a range of values. However, at exceptional values called bifurcation points, large shifts in the spike times were obtained in response to small changes in the stimulus and multiple spike patterns were revealed with an unsupervised method. Increasing the offset, which mimicked an increase in network activity, also increased the spike time reliability, but the spike times shifted earlier with increasing offset. Although the reliability was reduced at bifurcation points, the information about the stimulus time course was increased because each of the spike time patterns contained different information about the input.

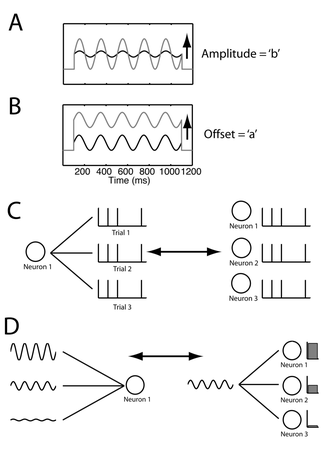

Figure 1. ***Conceptual framework for spike time patterns.*** Single cells were driven repeatedly in vitro by a current of the form I(t) = a + b h(t). The fluctuating term h(t) was a fixed realization of a correlated Gaussian process (Ornstein-Uhlenbeck process). (A) Variation of the amplitude, b. (B) Variation of the DC offset, a. (C) Repeated injection into a single cell on N trials (left) is equivalent to a single injection to a population of N independent cells (right). (D) Injection of the same waveform to independent cells with different electrical properties (capacitance, input resistance, right) is equivalent to injecting a single cell with currents having different values of a and b.

References

Bezdek, J. C. (1981). Pattern recognition with fuzzy objective function algorithms (New York, Plenum).

Fellous, J. M., Tiesinga, P. H., Thomas, P. J., and Sejnowski, T. J. (2004). Discovering spike patterns in neuronal responses. J Neurosci 24, 2989-3001.

Schreiber, S., Fellous, J. M., Tiesinga, P., and Sejnowski, T. J. (2004). Influence of ionic conductances on spike timing reliability of cortical neurons for suprathreshold rhythmic inputs. J Neurophysiol 91, 194-205.

Tibshirani, R., Walther, G., and Hastie, T. (2001). Estimating the number of clusters in a data set via the gap statistic. Journal of the Royal Statistical Society Series B-Statistical Methodology 63, 411-423.

Tiesinga, P., Fellous, J. M., and Sejnowski, T. J. (2008). Regulation of spike timing in visual cortical circuits. Nat Rev Neurosci.

Tiesinga, P. H. E., and Toups, J. V. (2005). The possible role of spike patterns in cortical information processing. Journal of Computational Neuroscience 18, 275-286.

Victor, J. D., and Purpura, K. P. (1996). Nature and precision of temporal coding in visual cortex: a metric-space analysis. J Neurophysiol 76, 1310-1326.

Wang, X. J., and Buzsaki, G. (1996). Gamma oscillation by synaptic inhibition in a hippocampal interneuronal network model. J Neurosci 16, 6402-6413.

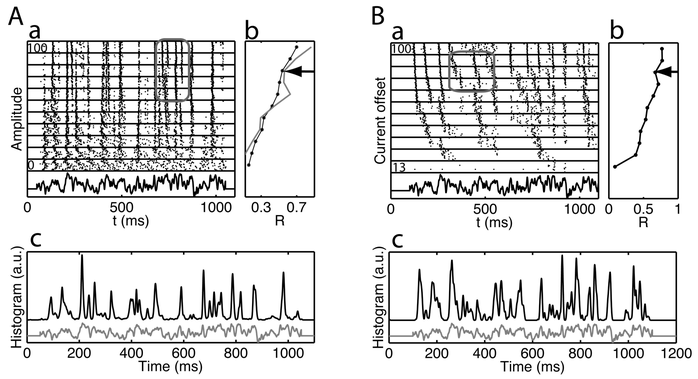

2

Figure 2. ***Spike timing in response to a fluctuating current is robust against changes in amplitude and offset.*** Responses of two Layer 5 pyramidal cells in a slice preparation of rat prefrontal cortex. (A) Variation in amplitude. (B) Variation in offset. Subpanel (a) rastergram, (b) reliability measure (sigma = 3 ms, see Schreiber et al.) (c) spike time histogram (averaged over parameter set). Arrows indicate local minima in reliability (B-b) or its derivative (A-b, gray curve) associated with a bifurcation point (boxes in A-a, B-a).

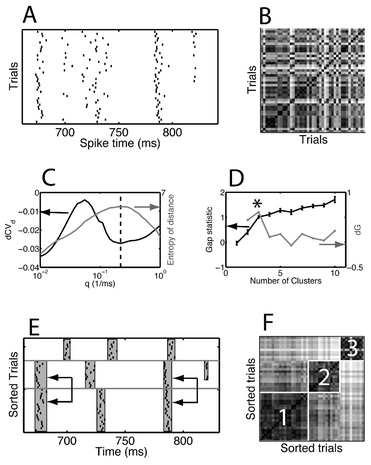

3

Figure 3. ***Method for detecting and characterizing spike timing events.*** (A) Sample rastergram of spike train data (200 ms window). (B) Distance matrix for the trials shown in panel A. The (i,j)th pixel is the Victor-Purpura distance (Victor & Purpura, 1996) between spike trains i and j for temporal resolution parameter q (ms). (C) Parameter q is chosen based on the resulting distance distribution, to maximize its entropy and minimize its log-differential coefficient of variation (dCV). Black curve, left-hand-side scale: dCV_q. Gray curve, right-hand-side scale: entropy of the distance distribution. (D) Number of spike patterns N_c was determined heuristically using the gap-statistic G(N_c) (Tibshirani et al., 2001) applied to a fuzzy clustering (FCM) algorithm (Bezdek, 1981; Fellous et al, 2004). Asterisk: The heuristic chooses N_c to maximize dG. (E) Rastergram of trials reordered by cluster membership. Horizontal lines separate clusters; vertical gray bands denote events. Arrows: events common to more than one cluster are merged. (F) Distance matrix for trials reordered by cluster membership.

Method summary: After choosing q and obtaining the VP distances between each pair of spike trains, the FCM algorithm is used to find N_c clusters in the data, after which the gap-statistic G(N_c) is computed. Each cluster is hypothesized to be a spike pattern. The gap-statistic measures the reduction of within cluster variance achieved by clustering relative to a similarly clustered surrogate data set with points uniformly distributed in the hypercube spanned by the range of the original data. The number of clusters is set to the maximum of the discrete derivative of G, i.e. $dG(N_c)=G(N_c)-G(N_c-1)$. Events common to more than one cluster are merged.

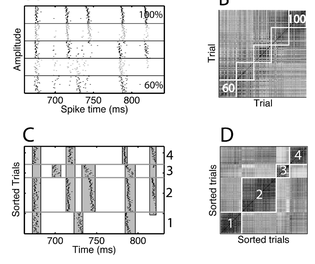

4

Figure 4. ***Bifurcation points lead to multiple spike patterns that persist across multiple amplitudes.*** The analysis procedure (see Figure 3) detected four clusters, each corresponding to a spike pattern. (A) Magnified rastergram from Figure 2, panel A-a. (B) Distance matrix for q=0.25 1/ms (see Figure 3).

(C) Rastergram with the trials sorted according to their cluster membership. Gray vertical bands correspond to detected events. (D) Distance matrix, sorted as in (C).

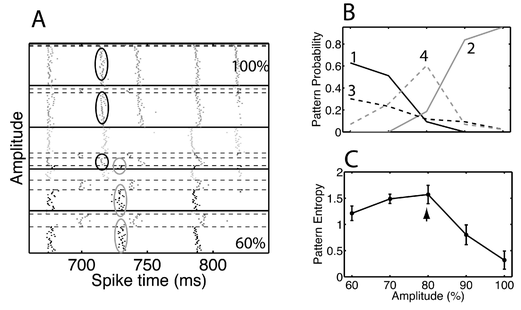

5

Figure 5. ***Decreasing spike time reliability was associated with changes in the pattern occupation.*** (A) Rastergram of the clustered data shown in Figure 4A. Blocks denote distinct amplitudes (separated by thick lines). Within each block, the trials are ordered based on their cluster membership (separated by thin dashed lines). Black ellipses: this event showed increasing reliability with amplitude. Gray ellipses: this event showed decreasing reliability with amplitude. (B) Pattern occupancy (probability) for an amplitude = the fraction of trials on which each pattern appears. Each of four patterns changes occupancy as amplitude varies. (C) Pattern diversity = entropy of the occupancy probability distribution. Peak diversity occurred at 80% amplitude (arrow). Error bars obtained via bootstrap.

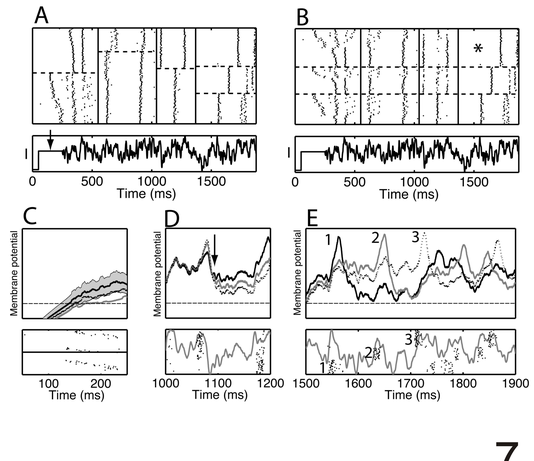

6

Figure 6. ***Spike patterns corresponded to voltage patterns.*** The single-amplitude data set was divided into four time segments. (A) Segment-by-segment rastergrams. In each segment trials were ordered according to the cluster membership in that segment. The clusters are separated by horizontal dashed lines, whereas segments are indicated by vertical lines. (B) Rastergram with trials in each segment ordered based on their cluster membership on the fourth segment (asterisk). At the bottom of A and B the current waveform is repeated for reference. There was a 200 ms long constant current step (arrow), whose amplitude took eleven different values (only one is shown). (C-E) The analysis procedure found 3 spike patterns in the fourth segment (between 1500 ms and 1900 ms), labeled 1 (solid black curve), 2 (dotted black curve), and 3 (gray curve). In each of the panels C-E, we show (top) the voltage traces averaged across all trials expressing that pattern (the y-axis covers the range from -65 to -35 mV) and (bottom) the current waveform together with a rastergram where the trials were ordered based on the cluster membership in the fourth segment. In (C) the gray bands indicate the plus or minus two standard error range for the black curve. The arrow in (D) indicates the point where differences between the voltage traces appeared.

7

Figure 7. ***Bifurcation points were observed in model simulations for amplitudes at which the spike count changed.*** Peaks in R-reliability coincided with plateaus in spike count (regions in which the trial-to-trial variability in spike count was small). Simulations applied the same current drive used in vitro to the Wang-Buzsaki model neuron (Tiesinga and Toups, 2005; Wang and Buzsaki, 1996). (A) R-reliability (sigma=1 ms) as a function of amplitude. Black and gray arrows: local minima in reliability corresponding to black and gray circled regions in (B). (B) Rastergram as a function of amplitude. Circles: examples of spike time bifurcation points. (C) R-reliability (gray curve) and mean spike count (black curve) versus amplitude. (D) R-reliability (gray curve) and standard deviation of spike count (black curve) versus amplitude. Double arrows in (C,D) denote peaks in reliability corresponding to plateaus in spike count (C) and minima in spike count variability (D).

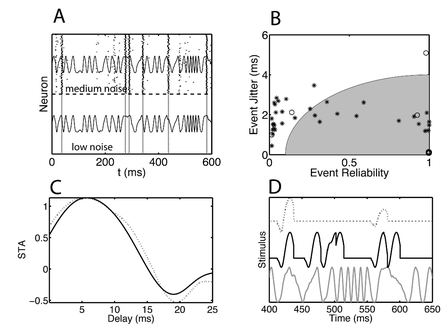

8

Figure 8. ***Information about the time course of the stimulus waveform is improved at bifurcation points because of the presence of multiple spike patterns.*** Comparison of low versus medium noise model neuron (Tiesinga and Toups, 2005). Stimulus reconstruction via spike-triggered average benefitted from moderate noise levels. (A) Rastergram for 100 trials of a low-noise (bottom) and medium-noise (top) model neuron (excerpt of a longer simulation). The low noise neuron spiked reliably in six events for every trial. The noisier neuron spiked less reliably, but exhibited additional events across trials. (B) R-reliability and jitter (standard deviation within an event) for each event for the entire stimulus duration (1100 ms). Open circles: low-noise results. Asterisks: medium-noise results. The gray-filled region represents the combination of jitter and reliability for which a putative postsynaptic neuron would generate a spike. (C) Spike-triggered average obtained across the entire stimulus period. Solid line: medium-noise neuron. Dotted line: low-noise neuron. (D) Stimulus waveform reconstructions. Dotted line: low-noise neuron. Black solid line: medium-noise neuron. Gray solid line: original stimulus waveform.

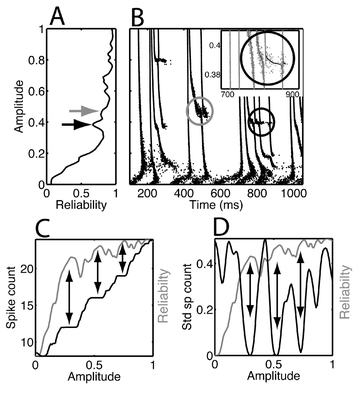

Conclusion

(1) In vitro data show evidence for bifurcation points, which correspond to a transient reduction in the R-reliability as a function of stimulus parameter.

(2) Bifurcation points could improve information content of spike trains because it combines spike times with an intermediate precision that is still high enough to be effective postsynaptically with an increase in the number of events thereby providing better coverage of the 'interesting' features of the stimulus time course.

Acknowledgements. This research was supported in part by the National Institutes of Health (R01-MH68481), start-up funds from the University of North Carolina at Chapel Hill, the Human Frontier Science Program and Radboud University Nijmegen. PJT was supported in part by NSF grant DMS-0720142. TJS was supported by the Howard Hughes Medical Institute.